Impact of Electrode Density and Configuration on EEG Source Localization of Visual Evoked Potentials

Master's Thesis

Panayiotis Paspalides

TU Delft

Impact of Electrode Density and Configuration on EEG Source Localization of Visual Evoked Potentials

by

Panayiotis Paspalides

(5987032)

Instructor:	Dr. ir. M.L. van de Ruit
Committee Members:	Dr. ir. R. van de Plas
	Dr. ir. B. Fereidoonnezhad
	Ir. I. Kyriazis
Project Duration:	Feb., 2025 - Sep., 2025
Institution:	Delft University of Technology
Faculty:	Faculty of Mechanical Engineering (ME), Delft
Laboratory:	NeuroMuscular Control Lab
Degree:	Master of Science in Biomedical Engineering: Neuromusculoskeletal Biomechanics
Presentation and Defense:	29 Sep 2025, 15:00 - 17:00

TU Delft

Acknowledgement

I am deeply grateful to my supervisor, Dr. ir. Mark van de Ruit, for his guidance, insightful feedback, and continuous support from the first outline to the final draft. His readiness to share knowledge and offer constructive advice whenever needed not only strengthened this project but also shaped my broader scientific approach. I also owe sincere thanks to my daily supervisor, Ir. Ioannis Kyriazis, whose eagerness to assist, practical suggestions, and hands-on help consistently guided me forward. His input was very useful in learning how to tackle research challenges with structure and creativity.

To my friends, those who stood by me before this journey began and those I had the privilege to meet over the past two years, thank you for the conversations, the laughs, and the motivation that kept me on track. You turned this journey into something truly worthwhile.

Finally, I owe the deepest thanks to my family. Your constant support, trust, and encouragement provided the foundation for this work. Thank you for your patience during the long days and for reminding me of the bigger picture. Without you, this thesis would not have been possible.

Panayiotis Paspalides
Delft, September 2025

Author's note: Parts of the text were refined with the assistance of ChatGPT 5 (OpenAI) to improve clarity and readability. All content, analyses and conclusions are the authors' own. AI tools were not used for data collection or analysis, and the author bears full responsibility for the final text.

Impact of Electrode Density and Configuration on EEG Source Localization of Visual Evoked Potentials

Panayiotis Paspalides
Supervisor: Dr. ir. M.L. van de Ruit

***Abstract*—This study investigates how electrode number and spatial configuration affect electroencephalography (EEG) source localization performance in the context of visual evoked potentials (VEPs). Five healthy participants performed visual stimulation tasks while EEG signals were recorded with a 256-channel cap. Six electrode montages were evaluated: four whole-head configurations (32, 64, 128, and 256 channels) and two targeted layouts (an 84-channel occipital-only montage and a 164-channel montage excluding frontal sensors). Source localization performance was assessed based on VEP neurophysiological expectations using three complementary indices: a Lateralization Index (LI) for hemispheric dominance, a Signal-to-Noise Ratio (SNR) at the source-space level, and a custom Occipital Precision Index (OPI) that quantifies how tightly activation is confined to occipital regions. Higher-density montages (128 and 256 channels) achieved the highest OPI values ($\geq$0.68), yielding the most focal localization and reflecting accurate activity confinement to the visual cortex. Notably, the targeted 84-channel occipital montage performed comparably to both the 128-channel whole-head and the 164-channel targeted configurations in OPI and SNR, demonstrating that dense sampling over the region of interest can rival broader higher-density coverage. In contrast, lower-density whole-head montages ($\leq$64 channels) exhibited inflated LI and SNR values but lower OPI, indicating reduced spatial precision despite seemingly higher signal metrics. The findings suggest that targeted electrode configurations can approach the performance of high-density caps when the region of interest is known in advance, though the small sample size (N=5) warrants caution and further validation.**

***Index Terms*—EEG source localization, Electrode density, Spatial sampling, Targeted montages, Visual evoked potentials.**

I. Introduction

A. Background and Motivation

EEG source localization is a powerful tool for non-invasively identifying the brain regions that generate electrical activity recorded on the scalp [1][2]. EEG offers higher temporal resolution than functional magnetic resonance imaging (fMRI) and, relative to magnetoencephalography (MEG), is less expensive and more widely available [3][4]. Yet, spatial resolution remains a key challenge for EEG. Due to volume conduction, signals originating from neural sources spread and mix as they pass through the brain, skull, and scalp tissues, which blurs the mapping from sources to electrodes [5]. This element is crucial in EEG source localization applications, for example, in the pre-surgical evaluation of epilepsy patients [6]. In this case, spatial resolution plays a decisive role in how accurately epileptogenic zones can be identified [7].

Delft University of Technology, Delft, 2628CD, The Netherlands;
e-mail: p.paspalides@student.tudelf.nl

In source localization, the spatial resolution is tightly linked to the electrode montage, which concerns the spatial arrangement and number of electrodes on an EEG cap. Typical EEG caps follow standardized montages that can be categorized into low-density configurations involving up to 32 electrodes, and high-density montages, usually ranging from 64 to 256 sensors [8][9].

In previous works, high-density EEG (hdEEG) systems with 64-256 channels have been shown to reduce localization error [10][11][12]. For example, one study on epileptic spike localization found that increasing from 32 to 64 electrodes improved the average localization error by 4 mm, going from 64 to 96 electrodes improved it by 1.3 mm, whereas moving from 96 to 128 electrodes the improvement was only 1 mm [13]. Nevertheless, despite the increasing number of reports supporting that a low electrode count can lead to higher localization errors, low-density montages such as the widely adopted international 10-20 system (19-21 electrodes) [14] have long served as a clinical standard for routine clinical use.

This can be attributed to the fact that hdEEG poses multiple practical barriers. High channel-count caps can be time-consuming to apply, as each electrode must be gelled and low impedance values must be ensured. This makes the experience more uncomfortable for the users and patients, and requires complex hardware and software that is often expensive [15][16]. For these reasons, low-density caps are considered to be more practical and are widely adopted. It has to be noted that alternative cap solutions that minimize or eliminate gel exist [17][18], but their equivalence for source localization has seen limited validation so far in the literature.

These challenges have motivated exploration of whether a strategically selected subset of electrodes targeted around regions of interest (ROIs) can maintain accuracy comparable to standardized hdEEG montages that are designed to uniformly spread across the entire head (whole-head montages). Limited prior research has hinted that focusing electrodes in the area of interest can preserve localization performance. For instance, recent work in epilepsy source imaging showed that using 25 core electrodes plus 8–11 additional electrodes around the seizure focus produced source solutions highly concordant with a full 83-channel montage. The authors reported a median source shift of only 13.2 mm between the targeted montage

and the 83-channel montage, with 93% of epileptic foci localized to the same sub-lobar region [19]. At the same time, other studies emphasize the importance of broad head coverage to avoid missing unexpected sources or incurring biases [20][21].

However, much of the existing work contrasts hdEEG with uniformly subsampled layouts. Direct tests of non-uniform, ROI-focused designs against whole-head configurations are scarce, so it remains unclear whether targeted placement can truly substitute for higher channel counts. This gap motivates the present study.

B. Aim and approach

This study aims to investigate how spatial sampling, defined by the number and configuration of electrodes in a montage, influences the source localization of visual evoked potentials (VEPs). This was tested by comparing six montage configurations: four standardized whole-head layouts (256, 128, 64, 32 channels) and two custom targeted layouts, the "only occipital" which concentrates 84 sensors only around the occipital region, and the "not frontal" (164 channels) which omits the frontal electrodes from the high-density cap.

This work extends prior literature by comparing not only different electrode densities and whole head versus targeted montages obtained by simple subsampling of higher density arrays. It also considers targeted montages whose spatial coverage over the ROIs differs from whole-head montages that may have more electrodes overall but provide sparser sampling of the ROIs. For example, a 128-channel montage that arranges sensors uniformly across the head can include more electrodes than the proposed custom "only occipital" montage (84 channels), yet the latter offers denser coverage of the ROI (the occipital lobe in this study). To the author's knowledge, this aspect has not yet been systematically addressed.

Furthermore, in contrast to the many studies that employ a localization error metric [22][23], this work assessed the localization performance of each montage with three complementary indices: Lateralization Index (LI), Signal-to-Noise ratio (SNR), and a custom Occipital Precision Index (OPI). LI was employed to determine the degree of contralateral versus ipsilateral occipital activation. This approach has been used in other EEG studies in which a lateralization index or asymmetry measure serves to quantify hemispheric dominance of the response [24][25]. The SNR metric was computed at the source-space level to compare the source activity to the baseline noise. This common measure is widely used as an indication of overall signal quality [26]. Finally, the custom Occipital Precision Index (OPI) was introduced as a way to measure how concentrated the activation is in the occipital ROIs compared to the activity "leaking" into adjacent regions. Even though this metric hasn't been observed in other works per se, conceptually it follows the idea behind the precision metric [27], treating activity inside the occipital ROIs as "true positives" and activity in adjacent non-occipital regions as "false positives". These indices were chosen because they can be interpreted based on expected VEP neurophysiological patterns and do not require an external ground truth such as fMRI scans.

C. Study Assumptions and Hypotheses

In the study, EEG data were recorded using a 256-channel EEG cap during lateralized and bilateral visual stimulation to obtain visual evoked potentials. VEPs constitute a useful testing modality because the cortical generators of their early components (C1 and P1) are well characterized. Component C1, which is defined as the first deflection of the VEP ($\sim$50–90 ms latency), is generated in the primary visual cortex ($\sim$Brodmann area (BA) 17), while the subsequent deflection known as component P1 ($\sim$80–120 ms) arises from adjacent extrastriate areas in the occipital lobe ($\sim$BAs 18 and 19) [28]. These components are typically maximal over occipital scalp electrodes and can demonstrate characteristic lateralization: for unilateral left-hemifield stimuli, the response is strongest over the right occipital scalp and vice versa [28][29][30]. Conversely, simultaneous bilateral visual stimulation is assumed to produce a roughly symmetric activation of both occipital lobes.

These neurophysiological expected patterns were used as an indirect ground truth for evaluating source localization results using the three indices described above. In particular, it was assumed that if a montage was to localize the VEP generators accurately, one would expect a strong bias towards the contralateral visual cortex for single hemifield stimuli, and a balanced activation for bilateral stimuli. If the montage performs poorly, the source estimates might appear more bilateral or even erroneously stronger on the ipsilateral side for hemifield stimuli, or show a strong imbalance when both hemifields are stimulated.

It was hypothesized that increasing electrode density would improve focal localization of occipital sources, and that a targeted montage with dense coverage over the occipital lobe could approach the performance of a higher-count uniform montage that spreads sensors across the entire head. In other words, dense sampling where it matters most (the occipital ROI) may be equally or even more valuable than uniformly sparse sampling the whole head, even if the total electrode count is higher in the latter case.

The remainder of the paper details the methodology, presents the results across montages and conditions, and discusses the implications and limitations of these findings.

II. Methodology

In this section, the complete study pipeline is documented so that the analysis can be reproduced. The participant sample, experimental setup and visual stimulation protocol are described. In addition, the preprocessing of EEG data and the investigated electrode montages are presented, along with the Source Localization process and performance metrics.

A. Participants and Data Acquisition

The study protocol was approved by the Human Research Ethics Committee (HREC) of TU Delft (Application number: 5615). In total, 5 healthy adults (3 males and 2 females, aged 20-30 years), participated in the experiment after providing informed consent.

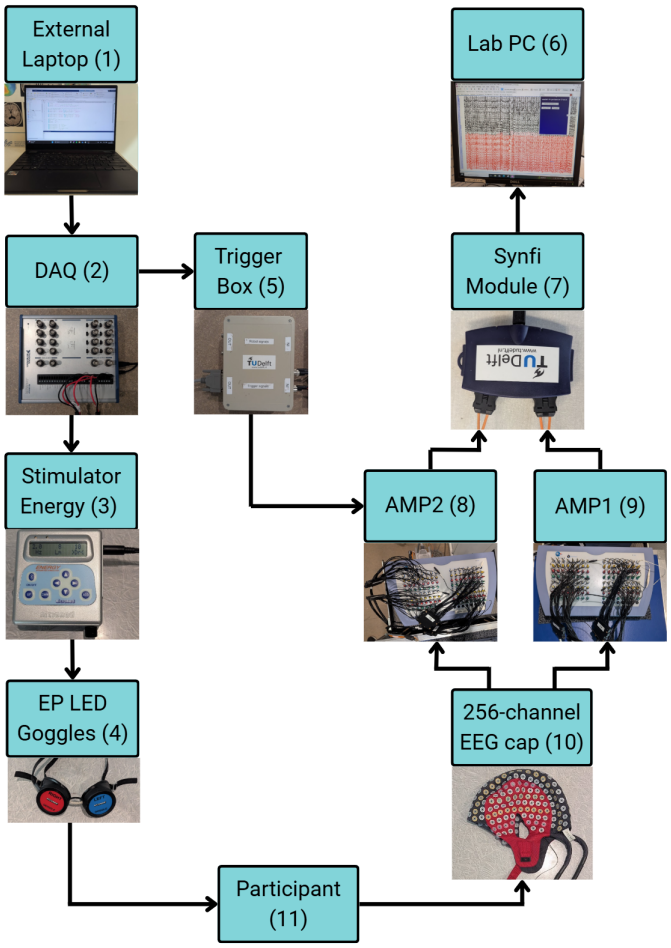

Fig. 1. Block diagram of the experimental setup hardware. An external laptop (1) runs the stimulation script and interfaces with the DAQ (2). The DAQ drives the stimulus generator (3) controlling the EP LED goggles (4) worn by the participant (11), and simultaneously sends event markers to a trigger box (5). Triggers are conveyed to both amplifiers (9,8), which record scalp EEG from the 256-channel cap (10). Amplifier data are streamed to the lab PC (6) via the Synfi module (7).

Figure 1 displays the experimental setup used for data acquisition.

To record scalp potentials, the high-density 256-channel Waveguard EEG cap (by ANT Neuro, model CA-126) was used. The cap was connected to a Refa system (by TMSi) with two 128-channel amplifiers coupled via fiber optic cables and a Synfi Module to the lab's acquisition computer. The two amplifiers shared a common reference electrode, and each used its own ground electrode, as recommended in the ANT Neuro asa-lab software manual. The EEG signals were sampled at 1024 Hz and monitored live during the experiments through the Asa-lab graphical user interface (GUI) software. Visual stimulation was delivered to the participants using a CE-marked LED goggle system consisting of the Intraoperative Nerve Stimulator Energy device along with the EP LED Goggles accessory (by Micromed). Additionally, an external laptop running a MATLAB script controlled the visual stimulation sequence and timing. As can be seen in Figure 1, the laptop was wired to a National Instruments NI USB-6361 data-acquisition device (DAQ). The DAQ was connected to both the Energy Stimulator for executing stimuli as specified by the stimulation script and to the amplifiers via a trigger box to mark the stimulus events. The triggers were forwarded to the Asa-lab software, thus marking the exact stimulus onset times and allowing precise epoching of the EEG data.

B. Visual Stimulation Protocol

Participants were seated in a darkened and soundproof room. The EP LED goggles used for providing the visual stimulation can present brief flashes to each eye and each visual hemifield separately. Consequently, 3 stimulation conditions were designed: Left Hemifield (LH), Right Hemifield (RH) and Both Fields (BF). In the left hemifield condition, a flash was delivered only to the temporal half of the left eye's visual field, which stimulates the nasal retina of the left eye and predominantly activates the right visual cortex[1]. In the right hemifield condition, the symmetric opposite was done for the right eye, thus stimulating the left visual cortex. In the both fields condition, a full field flash was presented to both eyes simultaneously, stimulating both the left and right visual pathways.

During the recordings, participants were instructed to keep their eyes closed and relax their facial muscles to minimize ocular and muscle artifacts. The eyes-closed instruction also served to prevent direct discomfort or blinking in response to the upcoming bright flashes presented via the goggles. Each flash had a duration of 10 ms. The flash intensity was set to the maximum of the Energy Stimulator device (8 lumens) to elicit robust brain responses. This choice is supported by prior findings that higher luminance yields larger visual evoked potential (VEP) amplitudes [31]. Stimuli were presented at random intervals with frequencies ranging from 1 to 1.6 Hz. Hence, the time interval between stimuli varied from 0.625-1 s, thus allowing time for the participant's brain to calm before providing the next stimulus. In addition, the random delays between consecutive stimuli were used to avoid any rhythmic adaptation or expectation effects that could occur with a fixed-interval stimulus sequence. The stimulus duration and inter-flash interval parameters were determined based on the recommendations of the standard clinical VEP guidelines given by the International Society for Clinical Electrophysiology of Vision (ISCEV standard, 2016 version) [32]. Each participant underwent 600 trials of each condition (1,800 flashes in total), delivered in 200-flash blocks lasting approximately 3 minutes each, with 1 minute of rest between blocks. This high trial count was chosen to ensure a high Signal-to-Noise Ratio (SNR) in the averaged VEPs. Three pilot tests were conducted to confirm that the chosen settings produced clear VEP peaks and that the participants could tolerate the stimulation comfortably. Including set-up, cap preparation, and recording, each session lasted approximately 4.5 hours per participant, with electrode gelling and impedance optimization accounting for the largest share of this time.

[1]A schematic representation of the anatomy of the human visual field is included in Appendix B

C. Impedance measurements

Before the start of each recording, all electrode sites were filled with conductive gel (High-Chloride Abrasive Electrolyte Gel by EASYCAP) to ensure low impedance contact with the scalp. During the cap preparation, individual electrode impedances were examined through the Asa-lab GUI. The threshold for maximum acceptable impedance was set at 20 kΩ. It should be noted that, for the first 2 participants, the 2 ground electrode leads stemming from each 128-channel amplifier were attached to the left and right mastoid areas of the participants. However, this placement caused several nearby cap electrodes (overlapping with the mastoids) to record poor EEG signals due to physical interference. Therefore, for the last 3 participants, the ground electrodes were repositioned to the participants' wrists, which substantially reduced the number of observed bad channels (fewer electrodes had to be excluded for flat/noisy signals).

D. EEG Preprocessing

EEG data were preprocessed using the MNE-Python package (v1.10.0) and custom Python scripts. Below, the main steps are listed in detail:

1. Flat EEG channels were identified and removed from the analysis.

2. Signals were then band-pass filtered from 0.5-40 Hz to remove slow drifts and high-frequency noise. The high-pass threshold was selected following the recommendation for EEG signal filtering in [33], while the low-pass boundary was determined considering that brain waves above 40 Hz were not expected to be relevant to the scope of the experiment.

3. Near identical channel signals (bridged channels) that were probably short-circuited due to excessive gelling were excluded. The bridged channel identification process was based on the computation of a channel-to-channel correlation matrix. Channel pairs with correlation ≥ 0.9999 were flagged and removed.

4. Bad/noisy channels were excluded in two phases. i) Automatic detection of channels whose standard deviation exceeded 5 times the median standard deviation across channels. ii) Manual removal of remaining noisy channels after visual inspection of the EEG signals.

5. To avoid imbalance in occipital coverage, if an electrode on or near the occipital region was removed on one hemisphere, the homologous electrode on the opposite hemisphere was also removed. This prevented unequal sensor counts that could bias results toward one side.

6. Clean EEG channels were assigned to 1 of the 6 montage configurations explained in detail in the following subsection II-E.

7. EEG signals were re-referenced to the common average after the montage assignment so that only channels included in that montage contributed to and received the average.

8. Subsequently, EEG data were segmented into epochs from -150 ms to +250 ms around each stimulus. Bad epochs were identified using a threshold method, where epochs containing signals with amplitude higher than $\pm$ 100 μV were dropped.

9. Clean epochs were then averaged to obtain a visual evoked potential for each participant, condition and montage.

E. Electrode Montages

During the preprocessing phase, EEG channels had to be assigned a montage configuration. In total, six different electrode montages were evaluated. Figure 2 illustrates the electrode counts and locations for each configuration, and categorizes them into whole-head uniform and targeted non-uniform montages.

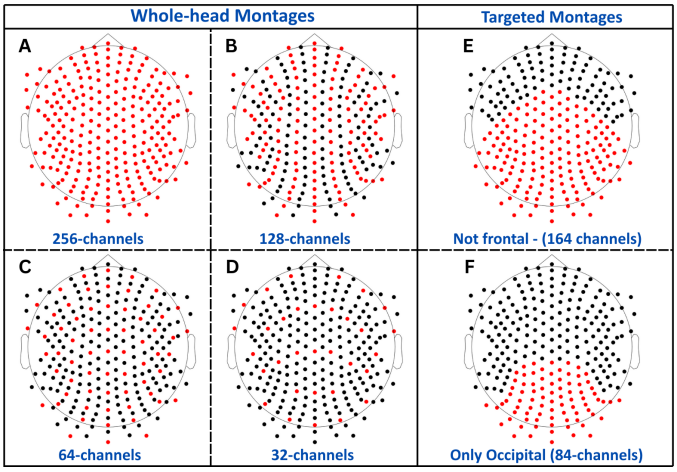

Fig. 2. Scalp maps illustrate the six montages derived from the 256-channel cap. In each panel, red dots mark electrodes included in the montage and black dots show available sites that were not used. Panels A–D depict uniform, whole-head subsets with 256, 128, 64, and 32 electrodes. Panel E shows the Not-frontal targeted montage (164 electrodes), which omits anterior sites while preserving the rest of the head coverage. Panel F shows the Only-occipital montage (84 electrodes) that concentrates sensors only over and around the occipital region.

The investigated montages displayed in Figure 2 are further explained below:

Figure 2.A (Whole-head, 256-channel): The complete set of electrodes covering the entire head following the Duke256 equidistant montage of the Waveguard EEG cap. This is the configuration with the highest density.

Figure 2.B (Whole-head, 128-channel): A subset of electrodes obtained by selecting every other line of electrodes from the 256 set in a manner that retained even coverage.

Figure 2.C (Whole-head, 64-channel): A further subset representing a standard mid-density EEG system approximating the layout of the 10-10 standardized system [34]. Again, the remaining channels were chosen so that all head regions had coverage.

Figure 2.D (Whole-head, 32-channel): A sparse montage akin to an extended 10-20 layout system [14]. In this subset the electrodes were distributed as evenly as possible to maintain at least some coverage across the entire head.

Figure 2.E ("Not frontal" Targeted, 164-channels): A custom high-density montage that included all the electrodes except those over the frontal pole and forehead. In total, 92 channels from the frontal area were removed from the entire 256 channel setup. This montage was included to examine

whether omitting sensors in a region far from the region of interest (occipital lobe) would have any effect on occipital source localization.

Figure 2.F ("Only Occipital" Targeted, 84-channels): A custom mid to high-density montage, focused on occipital area coverage. From the full-cap only 84 electrodes were selected, all located over the occipital and posterior parietal regions. It is important to note that even though this configuration has a smaller total electrode count compared to the 128-channel montage, the sensor density over the occipital lobe is actually higher. The rationale was to test whether concentrating the sensors where the signal is expected can compensate for the lack of global coverage.

F. Source Localization

The source localization procedure consisted of a forward model to compute the leadfield matrix and an inverse solution to estimate cortical activity.

1) Forward solution: Forward modeling was carried out using a template anatomical model as individual MRIs of the participants were not available. The "fsaverage" brain template from the FreeSurfer library was used as a canonical head. This template constitutes a combination of 40 MRI scans of real brains and provides an average cortical surface and geometry onto which source estimates can be mapped.

The EEG electrode coordinates were co-registered to the fsaverage head template by aligning anatomical landmarks (nasion, left and right preauricular points) and performing a surface-fit optimization using MNE-Python's co-registration GUI. The electrode coordinates on the head template were approximated using a modified version of the standardized electrode location file provided by the cap's manufacturer (ANT Neuro). This file follows the Duke256 equidistant layout and dictates the 3-dimensional space coordinates for each electrode on the 256-channel Waveguard cap. The file was adjusted to ensure sagittal plane symmetry of electrode positions in the occipital region, as it was discovered that the initial coordinates had minor asymmetries. In addition, all electrode positions were expanded radially by $20mm$ to achieve a better fit during subsequent co-registration with the head model. The same co-registration mapping file was used for all subjects, as it was assumed that the EEG cap was placed according to standard positions on each head.

To complete the forward model, a 3-layer boundary element model (BEM) was created from the fsaverage anatomy. The BEM included compartments for the scalp, skull, and brain. Standard conductivity values (0.3 S/m for scalp and brain, and 0.006 S/m for the skull) were selected as in [35][36]. The created source space consisted of 4098 dipole locations per hemisphere following an icosahedral subdivision grid. The final result showing the spatial alignment between the forward modeling parts (electrode locations, source space and head model) is shown in Figure 3.

Ultimately, the forward solution (leadfield matrix) was computed for all 6 different electrode-montages, each time taking into account only the corresponding electrodes comprising each montage.

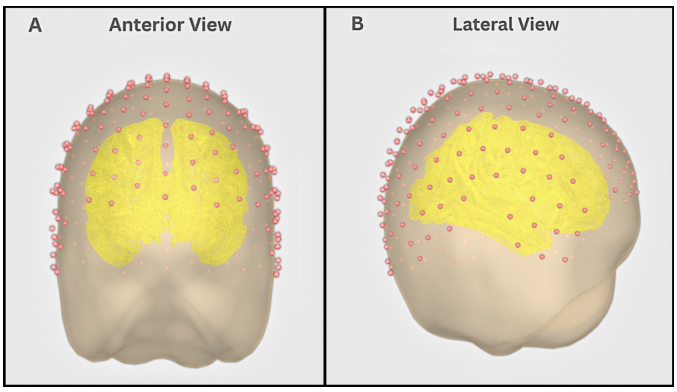

Fig. 3. Spatial alignment of forward modeling parts. Panels A (anterior view) and B (lateral view) show the EEG sensor positions (pink spheres) co-registered to the FreeSurfer fsaverage head template (beige surface), together with the source space (yellow vertices).

2) Inverse Solution: The standardized low-resolution brain electromagnetic tomography (sLORETA) [37] inverse method was employed to estimate cortical source activity from the scalp VEP data. The inverse operator was computed from the forward solution and a noise-covariance matrix[2], with regularization parameter [3] $\lambda^2 = 1/SNR = 9$, as a standard value of $SNR = 3$ was assumed for the averaged VEPs[38].

In total, 90 separate source localization cases were investigated (derived from 5(participants) · 3(conditions) · 6(montages) = 90) and the sLORETA source amplitude values were extracted for all cortical locations.

To avoid biasing the subsequent analysis to a fixed latency, no single post-stimulus time point was chosen to extract results. Instead, for each participant and condition, the VEP component (C1 or P1) exhibiting the clearest contralateral occipital response (for left/right hemifield stimulation condition) or the most balanced occipital activity (for both fields stimulation condition) was selected. In practice, the chosen component was identified based on the visual inspection of the participants' VEP and their occipital activity source amplitude. The selected components for each participant and condition are listed in Table I and served as the time-point around which the source localization results were examined to compare the performance of the various montages.

G. Regions of Interest (ROIs)

To analyze the source activity estimates in regions of interest (ROIs), the "PALS_B12_Brodmann" parcellation atlas was used. This atlas partitions the cortical surface into Brodmann areas (BA) and is compatible with the fsaverage brain model. A BA-based approach was adopted to facilitate comparison

[2]The noise-covariance matrix models how sensor noise is distributed and correlated across channels, and it is estimated from the pre-stimulus baseline of the VEPs. As a result, noisier channels are down-weighted and correlated noise is accounted for, making the inverse solution more stable.

[3]The linear inverse solves a trade-off: fit the data while keeping source amplitudes smooth. The regularization parameter sets the penalty strength for this trade-off. A larger λ^2 yields smoother, lower-amplitude maps while a smaller λ^2 yields sharper but noisier maps. Keeping a constant λ^2 across montages makes comparisons fair.

TABLE I
PARTICIPANT CHARACTERISTICS AND VEP COMPONENTS PER HEMIFIELD

Part. No.	Clean Channels	Clean Epochs	Condition	C1 Latency (ms)	P1 Latency (ms)	Selected Component
1	213	533	LH	62	98	P1
			RH	61	98	P1
			BF	52	87	P1
2	205	553	LH	64	83	C1
			RH	62	83	C1
			BF	60	83	C1
3	249	539	LH	53	73	P1
			RH	57	77	P1
			BF	53	75	P1
4	222	574	LH	59	69	P1
			RH	54	69	C1
			BF	73	75	C1
5	249	568	LH	62	80	P1
			RH	61	80	C1
			BF	60	106	C1

For each participant, the table lists the number of clean electrodes retained after preprocessing and the number of clean epochs used to produce the VEPs. For each stimulation condition (LH = Left Hemifield, RH = Right Hemifield, BF = Both Fields), the C1 and P1 columns report the mean peak latency (ms) averaged across all electrode montages identified for that participant. The "Selected Component" column indicates which component was used for subsequent analysis in that condition.

with previous VEP source studies that use the BA labeling system[28][39].

In particular, the areas taken into account for evaluating the performance of the various montage configurations include BA18, BA19, BA7 and BA39. Figure 4 illustrates those areas on the fsaverage brain surface.

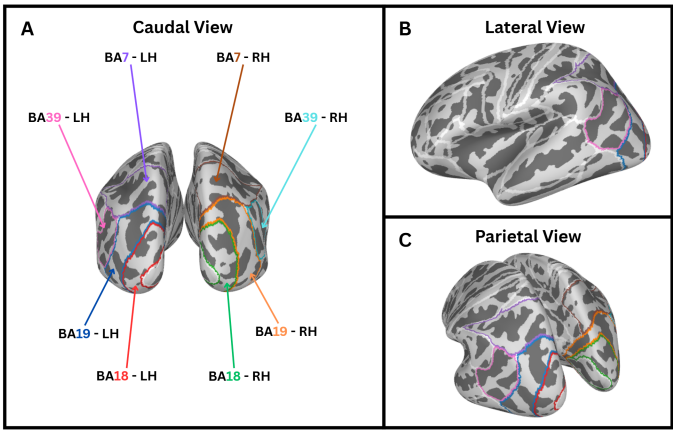

Fig. 4. Brodmann Areas 18, 19, 7 and 39 for each hemisphere (LH = Left Hemisphere, RH = Right Hemisphere) displayed on the fsaverage brain model. The activity in those areas was considered to compute the metrics and evaluate the performance of different montage configurations.

More specifically, the primary ROIs for this study were BA18 and BA19, which largely include the extrastriate visual cortex and correspond closely to V2 and adjacent areas (e.g. V3/V3a) in other common nomenclatures. However, note that BA labels and other visual field map conventions are not in one-to-one correspondence. Nevertheless, the reason for focusing on areas 18 and 19 was that component P1, which was initially assumed to be the main indicator of contralateral activity, reportedly originates from areas BA18 and BA19 [40][41][28].

Brain activity estimations spreading beyond the occipital ROIs were also investigated by examining BA7 and BA39, which belong to the parietal cortex. The activities estimated in these areas that directly surround the occipital regions of interest provided useful information as will be demonstrated in sections III and IV.

H. Performance Metrics

To compare how well expected brain activity was captured through each montage, 3 performance metrics were defined using the source amplitude maps obtained at the selected peak latency for each participant and condition (see Table I).

1) Lateralization Index (LI): This index quantifies the degree of left-right hemispheric asymmetry in the occipital source activity. LI was calculated based on the estimated values yielded by sLORETA and assigned to the sources comprising BA18 and BA19 of each hemisphere.

More specifically, for a given stimulation condition and component peak latency time t, LI was defined as,

$$\mathrm{LI}(t) = \frac{\left(A^{\mathrm{C}}_{18}(t) + A^{\mathrm{C}}_{19}(t)\right) - \left(A^{\mathrm{I}}_{18}(t) + A^{\mathrm{I}}_{19}(t)\right)}{\left(A^{\mathrm{C}}_{18}(t) + A^{\mathrm{C}}_{19}(t)\right) + \left(A^{\mathrm{I}}_{18}(t) + A^{\mathrm{I}}_{19}(t)\right)}, \quad (1)$$

where $A^{\mathrm{h}}_i(t)$ is the power percentage of Brodmann area i over the total brain power at time t. The superscript h denotes the hemisphere with respect to the stimulated visual hemifield (experiment condition). Superscript h can take the values of either C, or I, indicating the contralateral and ipsilateral hemisphere, respectively.

Power percentage $A^{\mathrm{h}}_i(t)$ was defined as,

$$\mathrm{A}^{\mathrm{h}}_{\mathrm{i}}(t) = \frac{Power^{\mathrm{h}}_i(t)}{\sum_{\mathrm{i}=1}^{52} Power^{\mathrm{C}}_i(t) + \sum_{\mathrm{i}=1}^{52} Power^{\mathrm{I}}_i(t)} \cdot 100 \quad (2)$$

where the number 52 used in the sum of the denominator corresponds to the total number of Brodmann areas, while $Power^{\mathrm{h}}_i(t)$ was computed using the following formula,

$$\mathrm{Power}^{\mathrm{h}}_{\mathrm{i}}(\mathrm{t}) = \sum_{\mathrm{s}=\mathrm{source}_{1_\mathrm{i}}}^{\mathrm{source}_{\mathrm{n_i}}} \mathrm{z_s(t)}^2, \quad (3)$$

The term $z_{\mathrm{s}}(t)$ represents the dimensionless standardized estimated value for source s at time t provided by the sLORETA algorithm following the source localization process. Each BA i is comprised by multiple sources in the source space, ranging from $source_{1_i}$ to $source_{n_i}$.

2) Occipital Precision Index (OPI): This metric assesses how focused the source activity is in the occipital ROIs (BA18 and BA19) versus the activity "leaking" into adjacent regions. As depicted in Figure 4, BA7 and BA39 are adjacent to the occipital lobe. Consequently, if the localized activity "leaks"

beyond BA18/19, it will often manifest in these neighboring parietal areas.

OPI is designed to complement the LI and capture the activity focality aspect that the LI misses. For a left and right hemifield stimulation conditions and component (C1/P1) peak latency time t, OPI was defined as,

$$\mathrm{OPI}(t) = \frac{A^{\mathrm{C}}_{18}(t)^2 + A^{\mathrm{C}}_{19}(t)^2}{A^{\mathrm{C}}_{18}(t)^2 + A^{\mathrm{C}}_{19}(t)^2 + A^{\mathrm{C}}_{7}(t)^2 + A^{\mathrm{C}}_{39}(t)^2} \quad (4)$$

For both fields stimulation condition and component (C1/P1) peak latency time t, OPI was defined as,

$$\mathrm{OPI}_{\mathrm{both}}(t) = \frac{A^{\mathrm{B}}_{18}(t) + A^{\mathrm{B}}_{19}(t)}{A^{\mathrm{B}}_{18}(t) + A^{\mathrm{B}}_{19}(t) + A^{\mathrm{B}}_{7}(t) + A^{\mathrm{B}}_{39}(t)}, \quad (5)$$

Where $A^{\mathrm{B}}_{i}(t) = A^{\mathrm{C}}_{i}(t)^2 + A^{\mathrm{I}}_{i}(t)^2$ accounting for occipital BA localization in both hemispheres. Again, for this condition, the superscripts C (contralateral) and I (ipsilateral) do not have a physical meaning, but during the computations, they corresponded to the left and right hemispheres, respectively.

3) Signal-to-Noise Ratio (SNR): LI and OPI metrics provide an anatomical and physiological understanding of the source localization results. In addition to that, the basic signal-to-noise ratio of the source estimates was evaluated. The idea was to quantify how much the source activity rises above the baseline noise level, and whether this is influenced by the montage configuration.

The source-space SNR was calculated as follows for each BA:

$$\mathrm{SNR}^{\mathrm{h}}_{\mathrm{i}}(t) = \frac{Power^{\mathrm{h}}_{i}(t)}{STD(\sum^{0}_{\mathrm{t}=-150} Power^{\mathrm{h}}_{i}(t))}, \quad (6)$$

Where $Power^{\mathrm{h}}_{i}(t)$ was defined in (3) and $STD(\sum^{0}_{\mathrm{t}=-150} Power_{i}(t)))$ corresponds to the standard deviation of the baseline $Power^{\mathrm{h}}_{i}$ of BA i. Baseline was defined as the pre-stimulus period between $t = -150ms$ and $t = 0ms$. Once again, superscript h denotes the investigated hemisphere, with terms C and I indicating the contralateral and ipsilateral hemisphere with respect to the hemifield stimulation condition.

For the left and right hemifield stimulation conditions, the averaged source-space SNR of contralateral BA 18 and 19 was computed for each participant and montage. For the both fields stimulation condition, the average SNR of BA 18 and 19 of both hemispheres was calculated.

Moreover, following a similar rationale to the one described for the OPI metric, it was decided to also calculate the corresponding SNR Precision Index (SNR-PI) metric. This metric helps evaluate whether certain montages yield cleaner source estimates in the expected regions, and not just generate higher SNR values by spreading estimated source activity to more sources.

For the left and right hemifield stimulation conditions and component (C1/P1) peak latency time t, this metric was defined as,

$$\mathrm{SNR-PI}(t) = \frac{SNR^{\mathrm{C}}_{18}(t) + SNR^{\mathrm{C}}_{19}(t)}{\sum_{k\in\{7,18,19,39\}} SNR^{\mathrm{C}}_{k}(t)}. \quad (7)$$

For both fields stimulation condition and component (C1/P1) peak latency time t, the SNR-PI was defined as,

$$\mathrm{SNR-PI}_{\mathrm{both}}(t) = \frac{SNR^{\mathrm{B}}_{18}(t) + SNR^{\mathrm{B}}_{19}(t)}{\sum_{k\in\{7,18,19,39\}} SNR^{\mathrm{B}}_{k}(t)}. \quad (8)$$

Where $SNR^{\mathrm{B}}_{i}(t) = SNR^{\mathrm{C}}_{i}(t) + SNR^{\mathrm{I}}_{i}(t)$ accounting for occipital BA in both hemispheres.

Again, only BA 18 and 19 were used in the numerator as they constitute the regions where the stronger "signal" is expected to be.

III. Results

A. Visual Evoked Potentials

VEP waveforms were obtained following the EEG preprocessing pipeline. Due to participants having their eyes closed during the experiment, the incidence of large artifacts was low. On average, 553 out of the 600 epochs collected per condition per participant remained to obtain the VEPs [4].

Figure 5 shows a representative VEP waveform of a participant for the RH stimulation condition. The colorful traces correspond to the 249 clean channels, while the early VEP components C1 and P1 are noted on the figure. For this particular case, component C1 was used to perform a further source localization analysis.

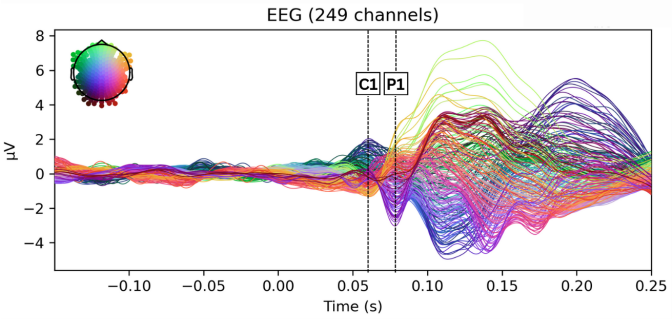

Fig. 5. Visual evoked potential from 249 clean electrodes during right hemifield stimulation condition. Each trace shows one channel (color indicates scalp position based on the top-left legend). The dashed vertical lines mark the C1 and P1 peak latencies.

B. Topographic maps

For all six investigated montages, Figure 6 shows the topographic maps obtained for component C1 of the same participant whose VEP is depicted in Figure 5. As these maps correspond to a right hemifield stimulation condition, the prominent activity appears contralaterally on the left occipital region. Higher-density layouts (Panels A, B) showed a more compact center of activity, whereas sparser layouts (C, D)

[4]Indicative VEPs from all participants are listed in Appendix A

displayed a broader spread of activity over posterior sensors. The targeted layouts (E, F) yielded a tight focus in the occipital ROI, but outside their coverage, the reconstructed activity does not appear consistent with physiological expectations. These maps provide a qualitative context for the source-space comparisons that follow.

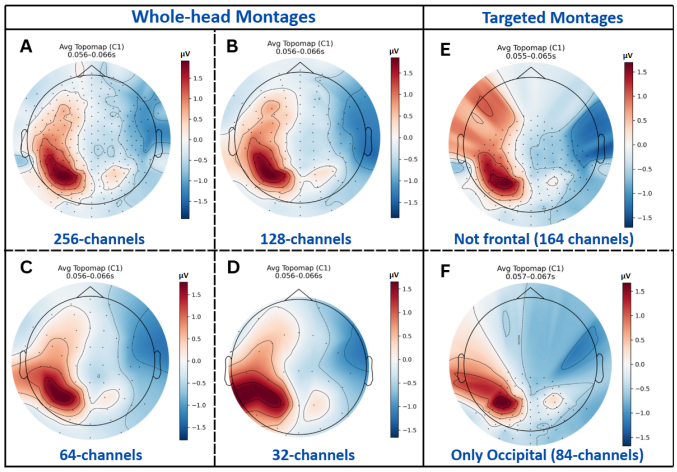

Fig. 6. Interpolated scalp voltage maps of the same participant averaged over ±5 ms around the C1 peak during right-hemifield stimulation condition. Panels A–D show uniform, whole-head montages (256, 128, 64, 32 channels), while panels E–F show targeted montages (Not frontal with 164 channels and Only-occipital with 84 channels). Dots mark electrode locations and contours indicate iso-voltage lines. The color bars give amplitude in µV, with warm colors positive and cool colors negative relative to the average reference. The figure enables visual comparison of how sensor density and coverage influence the sharpness and extent of the identified activity at C1.

C. Source localization group metrics

All metrics were first computed for each individual participant. To reduce sensitivity to very brief fluctuations, the source activity was averaged in a $10ms$ window centered on the chosen peak latency ($5ms$ before to $5ms$ after), thus obtaining a more stable estimate of peak activation.

The metrics were then averaged across the 5 participants to get a group mean and standard deviation for each montage and condition. These group results were used to compare the montages overall. Due to the small sample size, no formal statistical test was performed.

1) Lateralization Index: Figure 7 summarizes the group mean LI with standard deviations for each montage, plotted separately for Left, Right, and Both conditions. By definition, LI ranges from -1 to +1. An LI close to +1 indicates that almost all occipital activity (of BA 18 and 19) is estimated on the contralateral side, whereas an LI of 0 would indicate equal activity in both hemispheres, and a negative LI would indicate ipsilateral dominance.

As shown in Figure 7, the LI magnitude tended to increase when moving from 256 to 64 electrodes. For unilateral stimulation (Left and Right), LI appeared positive for almost all cases, indicating the expected contralateral occipital dominance. The main exception was the 32-channel montage, which showed the greatest overall variability and occasionally indicated ipsilateral dominance.

For the condition of bilateral field stimulation, the sign of LI is irrelevant, as both hemifields are stimulated and the expected "ground truth" would be a symmetric activation (LI value close to 0). Nevertheless, for the interpretation of this condition in Figure 7, a positive LI corresponds to left occipital hemisphere dominance, while a negative LI value shows dominant activity on the right occipital hemisphere.

2) Occipital Precision Index (OPI): Figure 8 displays the group OPI (mean ± SD) for each montage and condition. OPI is a unitless ratio with values ranging from 0 to 1, which effectively measures the fraction of contralateral activation that is confined to the core occipital visual areas. An OPI value of 1 means that all activity is estimated in BA18/19 (occipital ROIs) with none in BA7/39 (adjacent parietal regions). On the other hand, an OPI of 0 would mean no activity was identified in BA18/19.

From Figure 8, montages with denser sampling over the occipital lobe showed higher mean OPI values compared to sparser layouts. In particular, among whole-head montages, the ranking is identical across all conditions ($256 > 128 > 64 > 32$), while the targeted montages achieved overall mean OPI values closer to the 128-channel montage.

Notably, OPI should be interpreted only in a relative sense by comparing differences across montages rather than absolute values since the ground truth is unknown.

3) Signal-to-Noise Ratio (SNR): Figure 9 reports for each montage and condition the group source-space SNR (mean ± SD), indicating how strongly the peak source activity rises above the pre-stimulus baseline in the occipital ROIs (BA18/19).

As depicted in Figure 9, mean SNR increased as the number of sensors decreased, with the 32-channel montage showing the highest mean and standard deviation values across all conditions.

Figure 10 shows the group SNR-PI (mean ± SD), which applies the same logic as OPI but uses SNR values instead of activity amplitude. This helps evaluate whether any montage yields "cleaner" occipital estimates relative to adjacent parietal areas.

Based on Figure 10, SNR-PI is relatively stable across montages and conditions, with only small differences between configurations.

IV. Discussion

This study examined how spatial sampling, defined as the number and configuration of EEG electrodes, influences the source localization of visual evoked potentials based on known neurophysiological patterns. Six montages were compared, ranging from whole-head caps with 256, 128, 64, and 32 channels to two targeted layouts (an 84-channel occipital-only montage and a 164-channel not-frontal montage). The source localization performance of each configuration was evaluated using three complementary indices: Lateralization Index (LI), a custom Occipital Precision Index (OPI) and a source-space Signal-to-Noise Ratio (SNR).

Overall, the results indicate that montage selection has a clear impact on the evaluation indices, underscoring the importance of spatial sampling in source localization performance.

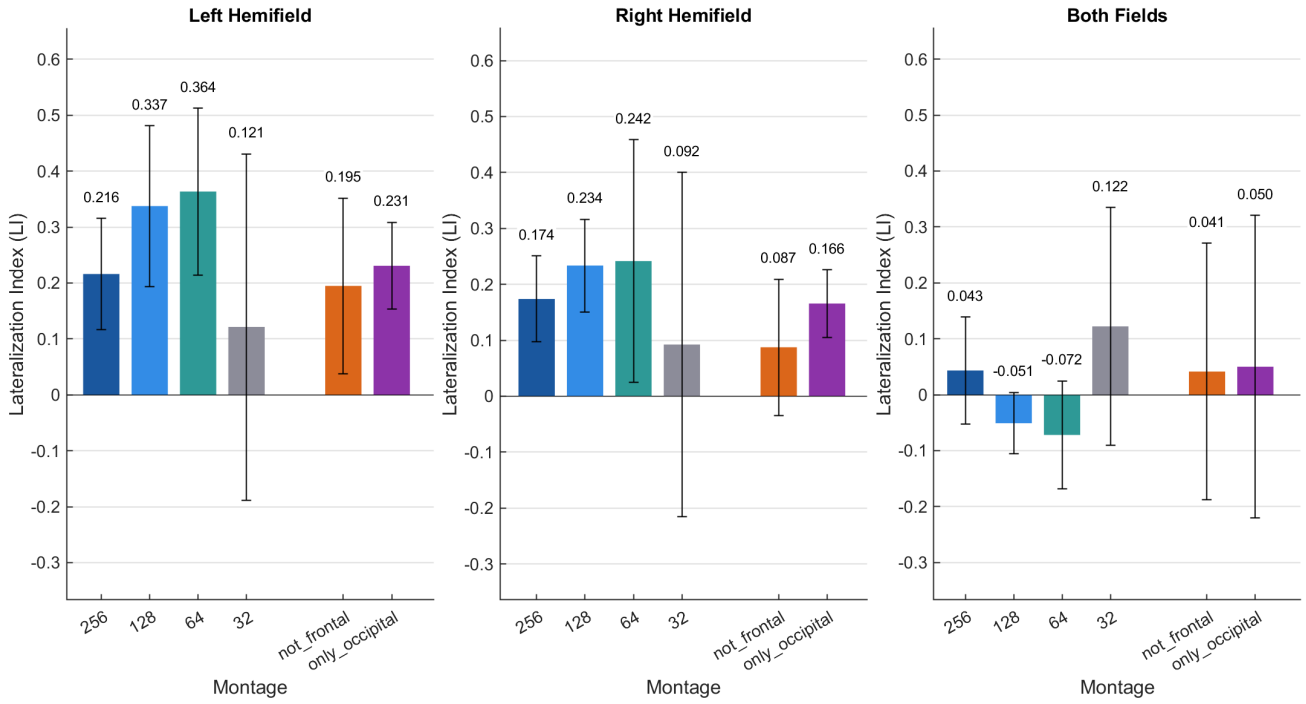

Fig. 7. Bars show the group ($N = 5$) mean lateralization index (LI) with standard-deviation error bars for each electrode montage, plotted separately for Left-hemifield, Right-hemifield, and Both-fields stimulation conditions. LI was computed from the source estimates at each participant's selected C1/P1 peak latency as stated in Table I. Positive LI values indicate contralateral dominance, negative values indicate ipsilateral dominance, and values near zero indicate balanced hemispheric activity. Uniform, whole-head coverage montages (256, 128, 64, 32) appear on the left of each panel, while non-uniform targeted montages (not frontal, only occipital) are shown on the right. Numeric labels above the bars report the group means.

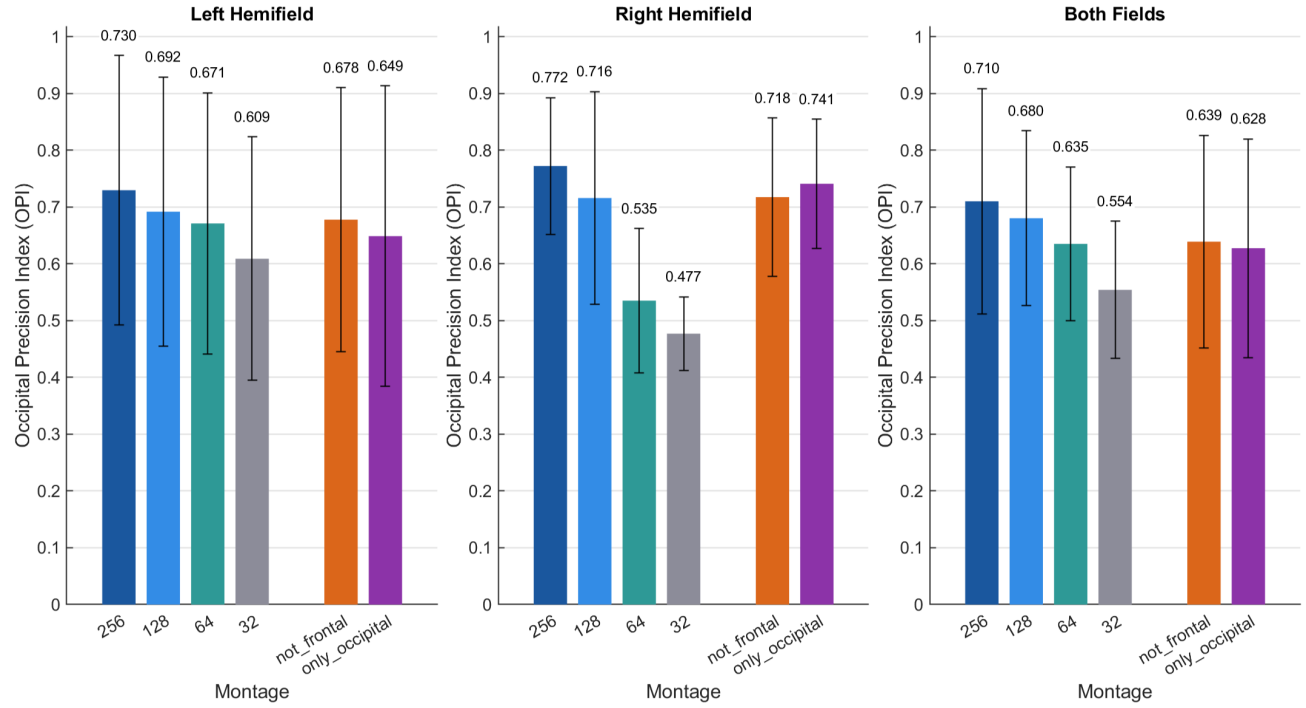

Fig. 8. Bars show the group ($N = 5$) mean Occipital Precision Index (OPI) with standard-deviation error bars for each electrode montage, displayed separately for Left-hemifield, Right-hemifield, and Both-fields stimulation conditions. OPI quantifies how tightly the activation is confined to occipital ROIs (BA18/BA19) relative to leaking into neighboring parietal regions (BA7/BA39). Values closer to 1 indicate more focal occipital localization, whereas lower values reflect broader spread beyond the occipital cortex. Uniform, whole-head montages (256, 128, 64, 32) are shown on the left of each panel, while non-uniform targeted montages (not frontal, only occipital) are shown on the right. Numeric labels above the bars report the group means.

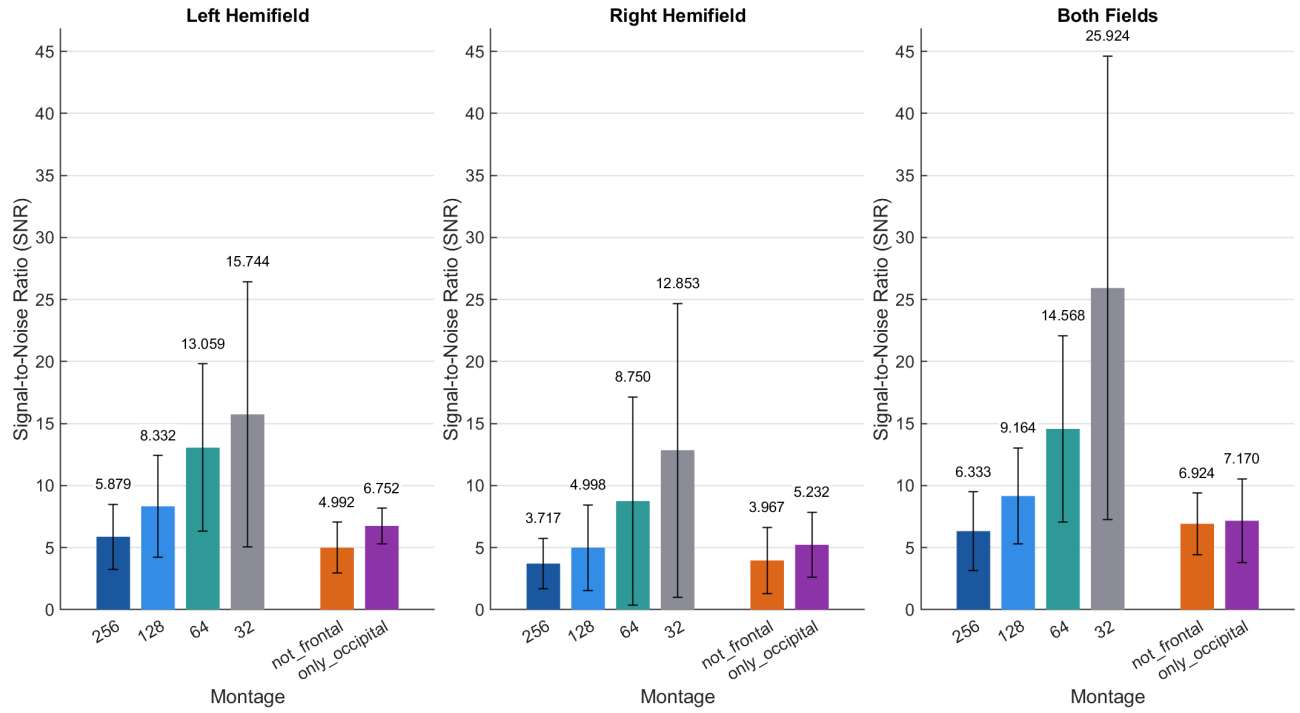

Fig. 9. Bars show the group ($N = 5$) mean source-space SNR with standard-deviation error bars for each electrode montage, plotted separately for Left-hemifield, Right-hemifield, and Both-fields stimulation conditions. SNR was computed for the combined ROIs BA18 and BA19. Larger SNR values indicate a stronger signal power relative to the standard deviation of the ROI's baseline. Uniform, whole-head montages (256, 128, 64, 32) appear on the left of each panel, while non-uniform targeted montages (not frontal, only occipital) are shown on the right. Numeric labels above the bars report the group means.

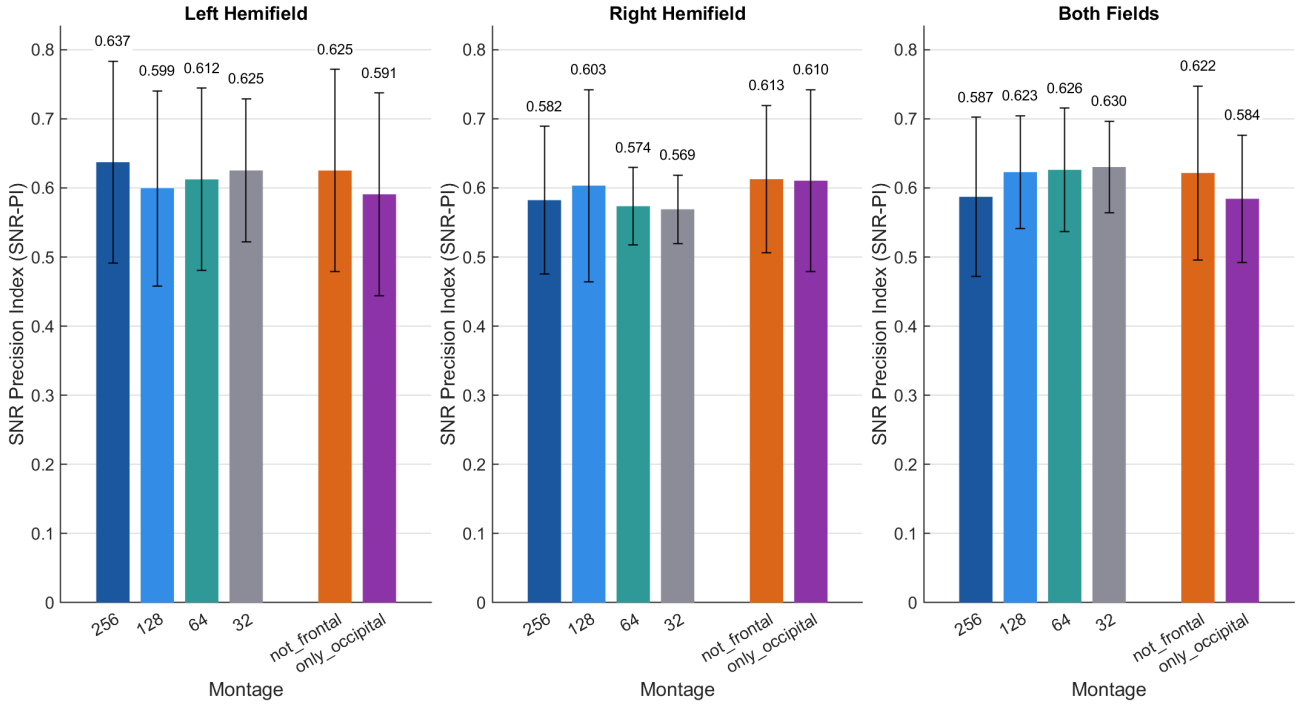

Fig. 10. Bars show the group ($N = 5$) mean SNR Precision Index (SNR-PI) with standard-deviation error bars for each electrode montage, displayed separately for Left-hemifield, Right-hemifield, and Both-fields stimulation conditions. SNR-PI quantifies how much the source-space SNR of occipital ROIs (BA18/BA19) increases relative to neighboring parietal regions (BA7/BA39) across montages. SNR-PI values increase when SNR in the occipital ROIs increases more compared to the SNR of adjacent regions and vice versa. Uniform, whole-head montages (256, 128, 64, 32) appear on the left of each panel, while non-uniform targeted montages (not frontal, only occipital) are shown on the right. Numeric labels above the bars report the group means.

Higher densities above 64 channels produced more focused occipital sources and aligned better with the expected patterns of the early VEP components C1/P1. By contrast, sparser montages with 32–64 channels sometimes yielded higher mean LI and SNR values than the 256-channel reference. However, as seen in the topographic (Figure 6) and later source maps (Figure 11), these higher values correspond to a broader spread of activity, rather than an improvement in localization performance. Quantitatively, this reduced focality effect is reflected by the lower OPI values of the lower-density montages.

Targeted montages that maintained dense sampling over the visual cortex produced sharply confined occipital activations and therefore high OPI. Both targeted layouts performed comparably to the whole-head setups: their OPI and SNR-PI indices were essentially on par with those of the 128-channel montage and similar to the 256-channel configuration.

These results suggest that a strategically targeted montage can preserve performance close to that of high-density whole-head configurations when the region of interest is sampled sufficiently. They also indicate that reducing the electrode count below about 64 sensors can inflate some localization metrics, a point that is examined in more detail later in the discussion.

A. Evaluation Framework

The evaluation framework sets the lens through which the results were interpreted. By design, in this study source localization performance relied on well-established neurophysiological response patterns and relative comparisons across montages rather than an external ground truth (e.g. fMRI localization). In particular, contralateral occipital dominance for unilateral stimulus conditions and symmetric occipital activation for bilateral stimuli were expected and used as a ground truth reference. Due to the small sample size ($N = 5$), no formal statistical tests were performed and thus, all comparisons are based on observed trends and magnitude differences rather than significance testing. The differences in mean and standard deviation values of the metrics across montage configurations are taken as indicators of relative source localization performance, acknowledging that true localization accuracy cannot be quantified without an established ground truth.

All metrics in this study (LI, OPI, SNR) are meaningful only as relative and not as absolute measures. For example, a higher OPI for one montage versus another suggests better localization focus for the expected region, but the absolute magnitude of these indices has no standalone significance without context. This is why in the analysis, normalized quantities such as OPI (Equation 4) and power percentages (Equation 2) instead of raw source magnitudes were utilized, in an attempt to allow for more fair comparisons of montage performance across participants.

First, differences between high-density and low-density electrode montages are discussed, and subsequently, the performance of uniform whole-head montages is compared to that of targeted montages.

B. High vs Low Density Montages

When comparing higher-density (128-256 channels) versus lower-density (32-64 channels) montages, a counterintuitive pattern emerged. The lower-density montages sometimes yielded higher values on certain metrics like the LI and source SNR compared to the high-density configurations. For example, in the LI group results (Figure 7), both the 32 and 64-channel montages occasionally showed a larger absolute LI magnitude than the 256-channel montage for each of the left and right stimulation conditions. Initially, one might interpret a higher LI as better localization of the expected contralateral activity. However, it is believed that in this context, it likely reflects an artifact induced by the reduced sensor count rather than a true improvement in localization. The rationale behind this interpretation is that with fewer electrodes, the source reconstruction algorithm has less spatial information and tends to spread the estimated activity over a broader cortical area. This interpretation is consistent with studies reporting that insufficient scalp sampling can lead to spatial aliasing and degradation of localization fidelity [42][20]. Consequently, when a low-density montage captures contralateral occipital activity, that activity can appear more intense in the source localization results as each electrode's data carry more weight over the occipital source-space neighborhood (fewer sensors share the load). This effectively boosts the total contralateral activation summed by the LI metric. By contrast, a high-density montage can confine the sensors' information more tightly to the source origin, resulting in a lower LI simply because the activation is more focal. In other words, reducing electrode count leads to a loss of spatial resolution, which can exaggerate metrics like LI without truly improving localization. This effect was visualized in the scalp topographies and source maps: as shown in Figure 6, the 256 and 128-channel montages produced a more compact occipital scalp potential map for the C1 component, whereas the 64 and 32-channel montages showed a progressively wider spread of activity over the scalp.

Similarly, the source localization comparison shown in Figure 11 illustrates how, for the same participant and condition, the localization of the 32-channel montage spreads the activity over a larger cortical area compared to the 256-channel solution. This result appears consistent with the idea of reduced spatial precision in low-density montages, as the 32-channel solution covers not only larger portions of the anticipated contralateral BA18 (orange) and 19 (blue), but also indicating intense activity into the adjacent BA7 (green) and BA39 (red).

Additionally, apart from the 32-channel configuration, all montages showed consistently positive LI values under unilateral stimulation, indicating contralateral occipital dominance. This aligns with the established contralateral pattern of early VEP components found in previous studies [28][29]. In contrast, the 32-channel montage demonstrated inconsistent and sometimes erroneous localization outcomes based on the LI metric (Figure 7). For instance, negative LI values signifying ipsilateral dominance were observed in unilateral stimulation. For the bilateral stimulus condition, the 32-channel montage

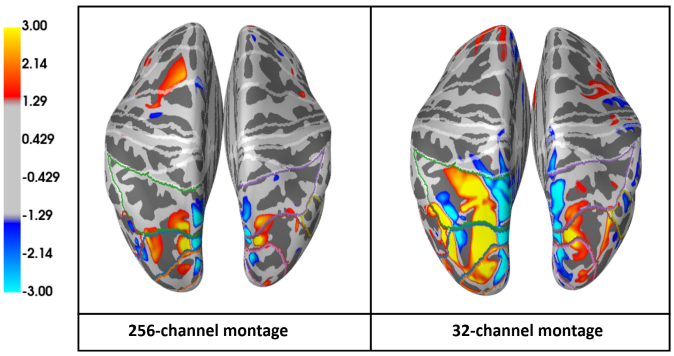

Fig. 11. Dorsal view of source localization results at the C1 peak (61 ms) during right-hemifield stimulation for the same participant as in Figures 5 and 6. The left panel shows the 256-channel montage and the right panel the 32-channel montage. The color bar on the left reports unitless sLORETA values. The side-by-side comparison illustrates how reducing electrode density changes the spatial extent and focality of the reconstructed occipital activation.

often produced a highly unbalanced LI (far from zero) with a mean value $= 12.2\%$, whereas the most imbalanced LI mean value out of the higher-density montages was only 5.1%, indicating a more balanced activation as anticipated. These discrepancies reinforce the idea that a high LI from a low-density montage does not equate to better localization performance. Instead it likely arises from the montage's inability to tightly localize the source, causing an overestimation of one side's activity.

The OPI results (Figure 8) seemed to also support the above interpretation. Across all conditions, OPI values tended to increase with electrode count, meaning higher-density montages localized a greater fraction of the activity within the core occipital regions (BA18/19). In contrast, low-density montages had lower OPI, consistent with more spread of activity outside the occipital ROI. Notably, the improvement in mean OPI value was most pronounced when moving from 32 to 64 or from 64 to 128 electrodes, with minimal gains beyond the 128 sensors. This trend is in line with established literature observations that show a plateau of localization error improvement as sensor density exceeds roughly 64–128 channels [4][20][21]. This suggests that OPI might have successfully captured the "resolution loss" effect described above, as the ranking order across the whole-head montages is consistent for all conditions. As montage density increases, OPI values increase as well, thus reflecting the tighter occipital focus that was visually evident in topographic (Figure 6) and source localization maps (Figure 11).

The source-space SNR metric showed a similar pattern to the LI, since mean SNR values based on occipital BA18/19 were consistently higher with fewer electrodes (Figure 9), while also displaying larger standard deviations. Once again, this can be attributed to the reduced spatial resolution of low-density montages. With sparse sampling, activity is assumed to spread and inflate the apparent signal in the ROI. To the knowledge of the author, no prior work directly reports higher source-space SNR values at lower channel counts as a consequence of signal dispersion.

In an attempt to test whether low-density montages actually yielded better quality localization, the SNR-based precision index (SNR-PI) was computed to compare the SNR of the occipital ROIs with the SNR of the neighboring parietal regions (BA7 and BA39). The group SNR-PI (see Figure 10) varied little across montages and conditions, indicating that low-density arrays raised the SNR values broadly rather than specifically in the occipital cortex where a stronger signal would be expected. This finding suggests that in practice, the occipital SNR increase observed in Figure 9 did not actually improve the contrast against the background activity, as all montages appear to offer the same level of relative SNR when comparing the ROIs to the neighbouring regions.

C. *Whole-Head vs Targeted Montages*

This study also examined whether targeted montages that concentrate sensors over the occipital ROI can perform comparably to uniform whole-head montages of similar or higher electrode count. Overall, the targeted configurations (84-channel "only occipital" and 164-channel "not frontal" montages) achieved similar results to the standard whole-head setups. Across the group, the two targeted montages showed mean LI, OPI, SNR and SNR-PI values in the same range as those of the 256 and 128-channel whole-head montages. In particular, for the "focality metrics" OPI and SNR-PI, targeted montages had nearly identical scores between the two, and showed equivalent results to high-density montages, especially the 128-montage. In the worst case across all conditions for the group OPI and SNR-PI metrics, the mean values between the two targeted montages varied by 3.8%, while both compared to the 128-montage varied just by 5.2%, and compared to the 256-montage by 8.2%. Importantly, the small difference between the two targeted layouts, despite the "not frontal" montage including nearly twice as many sensors as the "only occipital" montage, strongly suggests that dense ROI coverage might be more important for spatial sampling than the absolute number of electrodes.

The LI metric showed more variability for the targeted montages. Nevertheless, the LI mean values of the targeted montages were closer to the one of the 256-montage compared to the rest of the montages. This result might not be incidental as the 3 montages have the same spatial coverage over the occipital region and the highest across all montages. Consequently, this might once again imply that indeed, spatial coverage in the ROI where the activity appears is important, as a lower electrode count might cause activity to spread across sources and artificially boost the LI. These results support the initial hypothesis that densely sampling the region of interest can compensate for having fewer electrodes overall. By focusing electrodes over the visual cortex, the targeted montages maintained high spatial sampling where it mattered most, thus preserving the ability to identify the VEP generators. Hence, although the occipital montage uses only one-third the number of electrodes of the full 256, it does not lose much information within the visual cortex, which explains why its localization performance on occipital activity does not seem to lack compared to the higher-density configurations. This agrees with

the limited number of studies that compared targeted montages with higher-density configurations, reporting that ROI-focused layouts can reproduce similar HD-EEG source solutions with fewer sensors[19][36].

On the other hand, apart from the performance metrics, a closer inspection of the topographic maps (see Figure 6) showed that targeted montages do well at interpolating sensor signals inside the covered region, but struggling at the periphery and beyond. In both targeted montages, scalp voltage within the occipital region was mapped on par with the 256-channel montage. Notably, removing the frontal electrodes did not appear to influence the occipital voltage estimates. This observation is consistent with EEG sensitivity profiles, in which electrodes primarily capture activity from nearby cortex while sensitivity decreases with distance [43]. Nonetheless, at the edges of the sensor coverage, the limitations of the targeted approach became evident. With no electrodes present beyond a certain boundary, scalp voltages outside the border of the covered region were falsely calculated. This is seen in panels E and F of Figure 6, where the targeted montages showed voltage artifacts just outside their sensor range. The extent to which this phenomenon influences source localization results remains unknown as the source estimates of the anterior region were not examined in this study.

Despite these boundary issues, the targeted montages did not show large performance deficits on average. It should be noted, however, that they exhibited higher LI variance, in particular for the condition where both eyes and visual fields were stimulated simultaneously. In that case, the targeted montages produced approximately double the standard deviation across participants compared to the 256, 128 and 64-channel whole-head montages. A possible explanation for this behaviour is that bilateral stimulation activates a broader cortical region and pushes the targeted montage to its limits due to its restricted spatial coverage, hence delivering less accurate source localization results. However, this constitutes only a hypothesis which cannot be strongly supported especially due to the small participant sample size.

In summary, the comparison of whole-head versus targeted configurations indicates that strategically placing electrodes over a known region of interest can yield localization performance mostly comparable to a high-density cap covering the entire head. These findings align with previous targeted montage studies reporting that reducing the electrode number can be compensated by improving the spatial sensor arrangement [19][36]. This is an encouraging result for situations where reducing electrode count is desirable (e.g. to shorten preparation time, avoid patient discomfort or reduce costs), yet precise localization in a specific area is needed.

However, it should be stressed that the current study explicitly examined a scenario where the brain region generating the EEG signals was well known and was sufficiently covered by electrodes. Therefore, the findings discussed in this section depend on the fact that no sources lie outside the sensor-targeted area. If the actual neural generators extend beyond the assumed ROI, a targeted montage may estimate sources poorly or completely miss that activity. Consequently, targeted montages should be employed only when the region of interest is confidently identified in advance, and even then one must be mindful of edge coverage artifacts.

D. Limitations and Future Work

As with any experimental study, certain methodological constraints should be considered when interpreting the findings. One limitation concerns the total number of participants (N = 5). Although the dataset appeared to reveal consistent patterns across montage configurations, the small sample size prevents formal statistical testing and limits the extent to which the results can be generalized. The findings should therefore be regarded as suggestive trends rather than definitive effects. Expanding the participant pool in future work would allow for more robust statistical analyses and strengthen the external validity of the conclusions.

A second consideration is the inter-subject variability observed in the VEP responses (see Figure 14 in Appendix B). Group averages do not fully illustrate individual patterns such as differences in component morphology, amplitude and latency. This highlights the need for careful interpretation of group-level indices. Larger future samples and inter-subject analyses would help provide a clearer picture and separate systematic montage effects from individual differences.

Another limitation stems from the forward modeling approach. The present study used a template head model (“fsaverage”) and a standardized electrode location file for the co-registration process. Previous works have shown the importance of subject-specific head models in localization accuracy [22][2], as generic templates often introduce an offset between the model and the anatomy of each participant. Future work should therefore incorporate MRI-based head models and digitized electrode locations, as these measures could reduce model errors and enhance confidence in source localization results.

Additionally, the interpretation of the results is conditioned by the VEP component selection. As indicated in Table I, the chosen component for source localization analysis varied across participants and conditions. This was done so that the best indicator of hemispheric dominance was considered. The aim was not to compare C1 versus P1 per se, but to evaluate how well each montage captured contralateral activation, whichever component manifested it most clearly. However, since C1 and P1 may differ in their characteristics [28][29], component selection should be standardized in future work to enable more consistent group-level comparisons.

On a similar note, the ROI definition is another consideration. The source localization metrics focused on extrastriate occipital cortex (BA18/19) and adjacent parietal areas (BA7/39), but did not include BA17 (primary visual cortex), a known contributor to C1 [28]. To capture the C1 component in its entirety, future analyses should extend the ROI set to include BA17.

Finally, this study focused on six representative configurations (Figure 2), including two targeted layouts alongside four standard whole-head montages. While these choices capture key trade-offs between global and ROI coverage, they do not cover the full range of effective electrode arrangements.

Therefore, future work should explore a broader array of montage designs, including data-driven or algorithmic electrode selection methods as seen in [36], to identify configurations that maximize source localization performance.

V. Conclusion

This study examined the impact of electrode number and configuration on EEG source localization of visual evoked potentials (VEPs). To address this matter, an evaluation framework was developed that leverages expected VEP neurophysiological patterns together with complementary performance indices, thus eliminating the need for an external ground truth. Within this framework, the Occipital Precision Index (OPI) was introduced as a way to assess focality when the expected activity is well characterized. Using this approach, results confirmed that increasing electrode density in whole-head montages improved the focal localization of sources, aligning with earlier reports on the impact of sensor density. More importantly, targeted montages (84, 164 channels), designed for dense occipital ROI sampling, achieved localization performance comparable to uniformly spread high-density arrays (128, 256 channels), underscoring the potential of strategic electrode placement.

At the same time, lower-density montages (32, 64 channels) occasionally yielded inflated lateralization index (LI) and signal-to-noise ratio (SNR) values, but these increases reflected broader activity dispersion rather than genuine localization gains. The findings suggest that targeted layouts may help address practical constraints of high-density systems (e.g., preparation time, comfort, cost), provided the region of interest is established in advance. The consistency of results across all evaluation metrics (OPI, SNR, and LI) supports the credibility of these findings. However, the small sample size (N=5) limits the generalizability of the outcomes and future studies should validate these findings in larger cohorts. In summary, this work offers a structured evaluation framework for assessing montage trade-offs and highlights the potential of strategically targeted electrode configurations in applications where the expected source region is clearly defined.

References

[1] C. M. Michel, M. M. Murray, G. Lantz, S. Gonzalez, L. Spinelli, and R. G. De Peralta, "Eeg source imaging," *Clinical neurophysiology*, vol. 115, no. 10, pp. 2195–2222, 2004.

[2] R. Grech, T. Cassar, J. Muscat, K. P. Camilleri, S. G. Fabri, M. Zervakis, P. Xanthopoulos, V. Sakkalis, and B. Vanrumste, "Review on solving the inverse problem in eeg source analysis," *Journal of neuroengineering and rehabilitation*, vol. 5, no. 1, p. 25, 2008.

[3] S. Baillet, "Magnetoencephalography for brain electrophysiology and imaging," *Nature neuroscience*, vol. 20, no. 3, pp. 327–339, 2017.

[4] Y. Lu, G. A. Worrell, H. C. Zhang, A. Sohrabpour, and B. He, "Eeg source imaging and connectivity analysis in epilepsy patients," in *2013 Asilomar Conference on Signals, Systems and Computers*. IEEE, 2013, pp. 795–797.

[5] P. L. Nunez and R. Srinivasan, *Electric fields of the brain: the neurophysics of EEG*. Oxford university press, 2006.

[6] C. Baumgartner, J. P. Koren, M. Britto-Arias, L. Zoche, and S. Pirker, "Presurgical epilepsy evaluation and epilepsy surgery," *F1000Research*, vol. 8, pp. F1000–Faculty, 2019.

[7] F. Rosenow and H. Lüders, "Presurgical evaluation of epilepsy," *Brain*, vol. 124, no. 9, pp. 1683–1700, 2001.

[8] K. L. Lopez, A. D. Monachino, S. Morales, S. C. Leach, M. E. Bowers, and L. J. Gabard-Durnam, "Happilee: Happe in low electrode electroencephalography, a standardized pre-processing software for lower density recordings," *NeuroImage*, vol. 260, p. 119390, 2022.

[9] S. M. Stoyell, J. Wilmskoetter, M.-A. Dobrota, D. M. Chinappen, L. Bonilha, M. Mintz, B. H. Brinkmann, S. T. Herman, J. M. Peters, S. Vulliemoz *et al.*, "High-density eeg in current clinical practice and opportunities for the future," *Journal of clinical neurophysiology*, vol. 38, no. 2, pp. 112–123, 2021.

[10] V. Brodbeck, L. Spinelli, A. M. Lascano, M. Wissmeier, M.-I. Vargas, S. Vulliemoz, C. Pollo, K. Schaller, C. M. Michel, and M. Seeck, "Electroencephalographic source imaging: a prospective study of 152 operated epileptic patients," *Brain*, vol. 134, no. 10, pp. 2887–2897, 2011.

[11] M. Odabaee, W. J. Freeman, P. B. Colditz, C. Ramon, and S. Vanhatalo, "Spatial patterning of the neonatal eeg suggests a need for a high number of electrodes," *Neuroimage*, vol. 68, pp. 229–235, 2013.

[12] N. Kuhnke, J. Schwind, M. Dümpelmann, M. Mader, A. Schulze-Bonhage, and J. Jacobs, "High frequency oscillations in the ripple band (80–250 hz) in scalp eeg: higher density of electrodes allows for better localization of the seizure onset zone," *Brain topography*, vol. 31, no. 6, pp. 1059–1072, 2018.

[13] A. Sohrabpour, Y. Lu, P. Kankirawatana, J. Blount, H. Kim, and B. He, "Effect of eeg electrode number on epileptic source localization in pediatric patients," *Clinical Neurophysiology*, vol. 126, no. 3, pp. 472–480, 2015.

[14] J. HH, "The ten-twenty electrode system of the international federation," *Electroenceph clin Neurophysiol*, vol. 10, pp. 367–380, 1958.

[15] S. M. Safavi, B. Lopour, and P. H. Chou, "Reducing the computational complexity of eeg source localization with cortical patch decomposition and optimal electrode selection," *IEEE Transactions on Biomedical Engineering*, vol. 65, no. 10, pp. 2298–2310, 2018.

[16] J. G. Ochoa, J. Rini, J. Diaz, and J. Botwell, "Technical description of long-term high-density eeg monitoring using 128-channel cap applied with a conductive paste," *Journal of Clinical Neurophysiology*, vol. 36, no. 3, pp. 175–180, 2019.

[17] M. Topor, B. Opitz, and P. J. Dean, "In search for the most optimal eeg method: A practical evaluation of a water-based electrode eeg system," *Brain and neuroscience advances*, vol. 5, p. 23982128211053698, 2021.

[18] K. E. Mathewson, T. J. Harrison, and S. A. Kizuk, "High and dry? comparing active dry eeg electrodes to active and passive wet electrodes," *Psychophysiology*, vol. 54, no. 1, pp. 74–82, 2017.

[19] A. Horrillo-Maysonnial, T. Avigdor, C. Abdallah, D. Mansilla, J. Thomas, N. von Ellenrieder, J. Royer, B. Bernhardt, C. Grova, J. Gotman *et al.*, "Targeted density electrode placement achieves high concordance with traditional high-density eeg for electrical source imaging in epilepsy," *Clinical Neurophysiology*, vol. 156, pp. 262–271, 2023.

[20] J. Song, C. Davey, C. Poulsen, P. Luu, S. Turovets, E. Anderson, K. Li, and D. Tucker, "Eeg source localization: Sensor density and head surface coverage," *Journal of neuroscience methods*, vol. 256, pp. 9–21, 2015.

[21] G. Lantz, R. G. De Peralta, L. Spinelli, M. Seeck, and C. Michel, "Epileptic source localization with high density eeg: how many electrodes are needed?" *Clinical neurophysiology*, vol. 114, no. 1, pp. 63–69, 2003.

[22] Z. Akalin Acar and S. Makeig, "Effects of forward model errors on eeg source localization," *Brain topography*, vol. 26, no. 3, pp. 378–396, 2013.

[23] J. Rong, R. Sun, Y. Guo, and B. He, "Effects of eeg electrode numbers on deep learning-based source imaging," in *International Conference on Brain Informatics*. Springer, 2023, pp. 123–132.

[24] S. Tune, M. Alavash, L. Fiedler, and J. Obleser, "Neural attentional-filter mechanisms of listening success in middle-aged and older individuals," *Nature Communications*, vol. 12, no. 1, p. 4533, 2021.

[25] R. H. Van der Lubbe and C. Utzerath, "Lateralized power spectra of the eeg as an index of visuospatial attention," *Advances in cognitive psychology*, vol. 9, no. 4, p. 184, 2013.

[26] A. Ali, R. Afridi, T. A. Soomro, S. A. Khan, M. Y. A. Khan, and B. S. Chowdhry, "A single-channel wireless eeg headset enabled neural activities analysis for mental healthcare applications," *Wireless Personal Communications*, vol. 125, no. 4, pp. 3699–3713, 2022.

[27] D. M. Powers, "Evaluation: from precision, recall and f-measure to roc, informedness, markedness and correlation," *arXiv preprint arXiv:2010.16061*, 2020.

[28] F. Di Russo, A. Martínez, M. I. Sereno, S. Pitzalis, and S. A. Hillyard, "Cortical sources of the early components of the visual evoked potential," *Human brain mapping*, vol. 15, no. 2, pp. 95–111, 2002.

[29] H. Takemura, K. Yuasa, and K. Amano, "Predicting neural response latency of the human early visual cortex from mri-based tissue measurements of the optic radiation," *eneuro*, vol. 7, no. 4, 2020.
[30] S. P. Kelly, M. I. Vanegas, C. E. Schroeder, and E. C. Lalor, "The cruciform model of striate generation of the early vep, re-illustrated, not revoked: A reply to ales et al.(2013)," *NeuroImage*, vol. 82, pp. 154–159, 2013.
[31] K. Eroğlu, T. Kayıkçıoğlu, and O. Osman, "Effect of brightness of visual stimuli on eeg signals," *Behavioural Brain Research*, vol. 382, p. 112486, 2020.
[32] J. V. Odom, M. Bach, M. Brigell, G. E. Holder, D. L. McCulloch, A. Mizota, A. P. Tormene, and I. S. for Clinical Electrophysiology of Vision, "Iscev standard for clinical visual evoked potentials:(2016 update)," *Documenta Ophthalmologica*, vol. 133, no. 1, pp. 1–9, 2016.
[33] A. Delorme, "Eeg is better left alone," *Scientific reports*, vol. 13, no. 1, p. 2372, 2023.
[34] G.-E. Chatrian, E. Lettich, and P. L. Nelson, "Modified nomenclature for the "10%" electrode system1," *Journal of Clinical Neurophysiology*, vol. 5, no. 2, pp. 183–186, 1988.
[35] E. Mikulan, S. Russo, S. Parmigiani, S. Sarasso, F. M. Zauli, A. Rubino, P. Avanzini, A. Cattani, A. Sorrentino, S. Gibbs *et al.*, "Simultaneous human intracerebral stimulation and hd-eeg, ground-truth for source localization methods," *Scientific data*, vol. 7, no. 1, p. 127, 2020.
[36] A. Soler, L. A. Moctezuma, E. Giraldo, and M. Molinas, "Automated methodology for optimal selection of minimum electrode subsets for accurate eeg source estimation based on genetic algorithm optimization," *Scientific reports*, vol. 12, no. 1, p. 11221, 2022.
[37] R. D. Pascual-Marqui *et al.*, "Standardized low-resolution brain electromagnetic tomography (sloreta): technical details," *Methods find exp clin pharmacol*, vol. 24, no. Suppl D, pp. 5–12, 2002.
[38] S. Baillet, J. Mosher, and R. Leahy, "Electromagnetic brain mapping," *IEEE Signal Processing Magazine*, vol. 18, no. 6, pp. 14–30, 2001.
[39] A. Martinez, L. Anllo-Vento, M. I. Sereno, L. R. Frank, R. B. Buxton, D. Dubowitz, E. C. Wong, H. Hinrichs, H. J. Heinze, and S. A. Hillyard, "Involvement of striate and extrastriate visual cortical areas in spatial attention," *Nature neuroscience*, vol. 2, no. 4, pp. 364–369, 1999.
[40] V. P. Clark, S. Fan, and S. A. Hillyard, "Identification of early visual evoked potential generators by retinotopic and topographic analyses," *Human brain mapping*, vol. 2, no. 3, pp. 170–187, 1994.
[41] C. Miniussi, M. Girelli, and C. A. Marzi, "Neural site of the redundant target effect: Electrophysiological evidence," *Journal of cognitive neuroscience*, vol. 10, no. 2, pp. 216–230, 1998.
[42] R. Srinivasan, D. M. Tucker, and M. Murias, "Estimating the spatial nyquist of the human eeg," *Behavior Research Methods, Instruments, & Computers*, vol. 30, no. 1, pp. 8–19, 1998.
[43] R. Srinivasan, W. R. Winter, J. Ding, and P. L. Nunez, "Eeg and meg coherence: measures of functional connectivity at distinct spatial scales of neocortical dynamics," *Journal of neuroscience methods*, vol. 166, no. 1, pp. 41–52, 2007.
[44] Perellonieto, "Human visual pathway," 2016, cC BY-SA 4.0, via Wikimedia Commons. [Online]. Available: https://commons.wikimedia.org/wiki/File:Human_visual_pathway.svg

APPENDIX A

TABLE II
LIST OF ABBREVIATIONS

Abbreviation	Definition
EEG	Electroencephalography
VEP	Visual Evoked Potential
ROI	Region of Interest
BA	Brodmann Area
fMRI	Functional Magnetic Resonance Imaging
MEG	Magnetoencephalography
hdEEG	High-Density Electroencephalography
LI	Lateralization Index
SNR	Signal-to-Noise Ratio
OPI	Occipital Precision Index
SNR-PI	Signal-to-Noise Ratio Precision Index
GUI	Graphical User Interface
DAQ	Data Acquisition (device)
LH	Left Hemifield
RH	Right Hemifield
BF	Both Fields
HREC	Human Research Ethics Committee
BEM	Boundary Element Model
MRI	Magnetic Resonance Imaging
sLORETA	Standardized Low-Resolution Brain Electromagnetic Tomography
ISCEV	International Society for Clinical Electrophysiology of Vision
STD	Standard Deviation

APPENDIX B

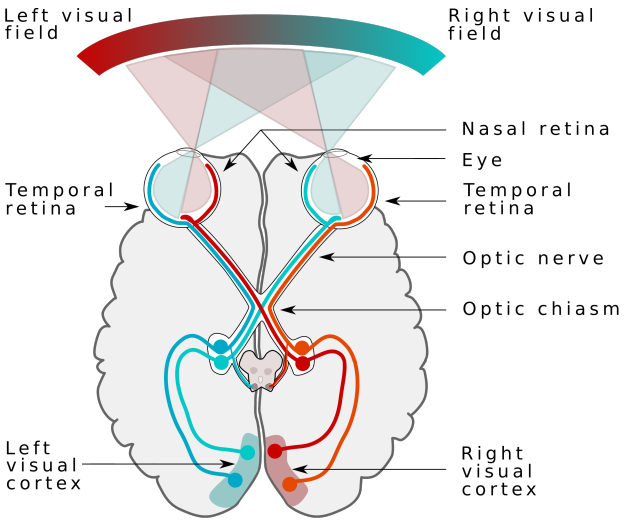

Fig. 12. Simplified representation of the human visual system illustrating the visual fields and pathways from the eyes to the visual cortex. (Modified from [44]).

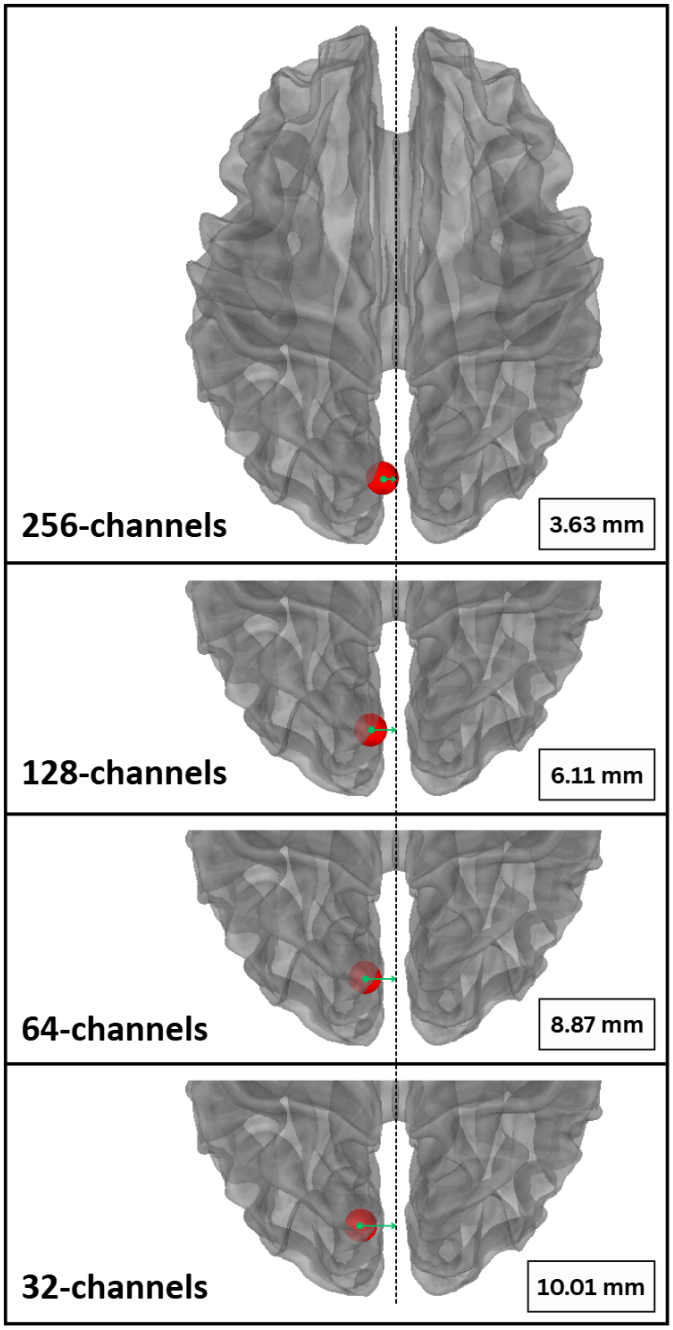

Fig. 13. Center-of-mass (CoM) of occipital/parietal activity across montages. For each montage (256, 128, 64, 32 channels), the CoM was computed over bilateral BA18, 19, 7 and 39 and displayed on a dorsal view of the source space (transparent gray). The red sphere marks the CoM of estimated activity under right-hemifield stimulation condition, which appears contralaterally in the left visual cortex. Green arrows indicate the horizontal distance from the midline (dashed line). The distance value in millimeters is stated in the boxed label at the bottom right corner of each montage panel. The progressive increase in distance with lower sensor density visually reflects the inflation of contralateral activity captured by the Lateralization Index. These results correspond to the same participant and condition as in Figures 5, 6 and 11.

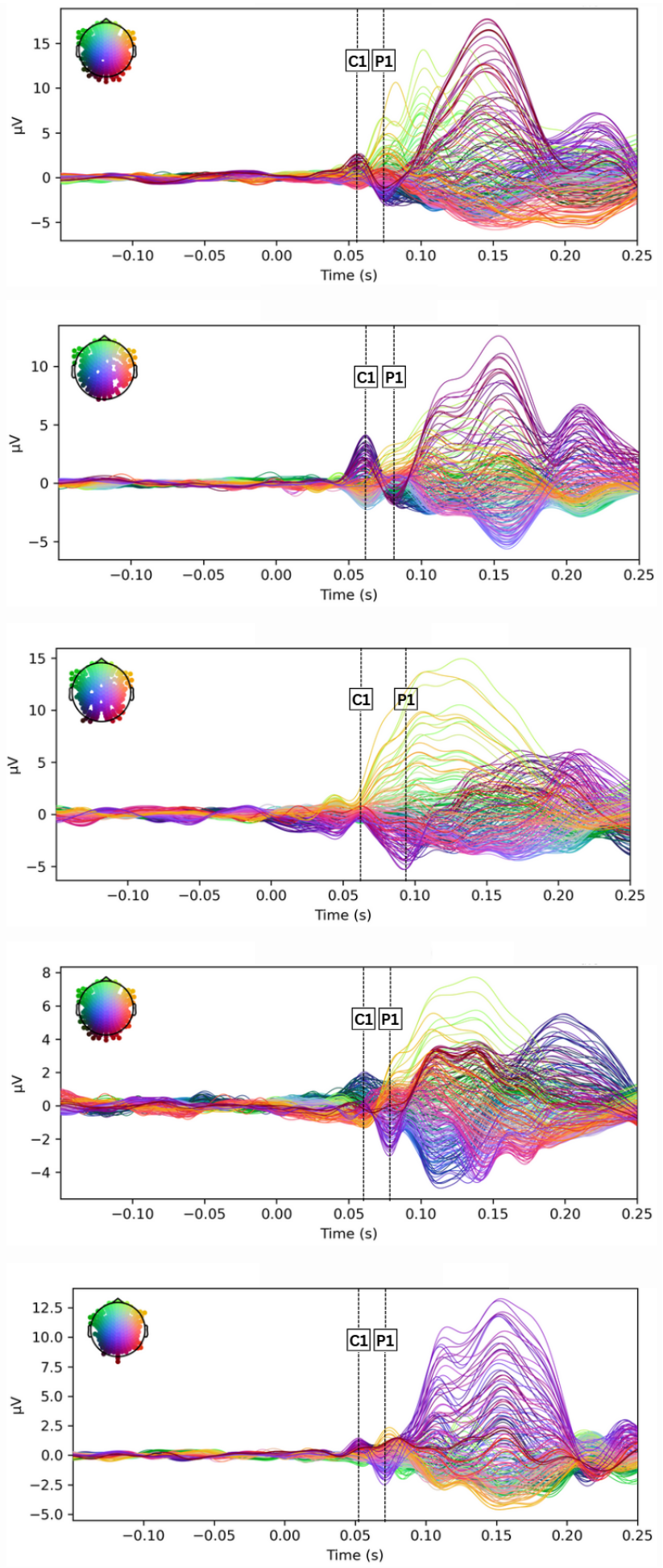

Fig. 14. Indicative VEPs from all participants under the right hemifield stimulation condition using the 256-channel montage. Each trace shows one channel (color indicates scalp position based on the top-left legend). The dashed vertical lines mark the C1 and P1 peak latencies.

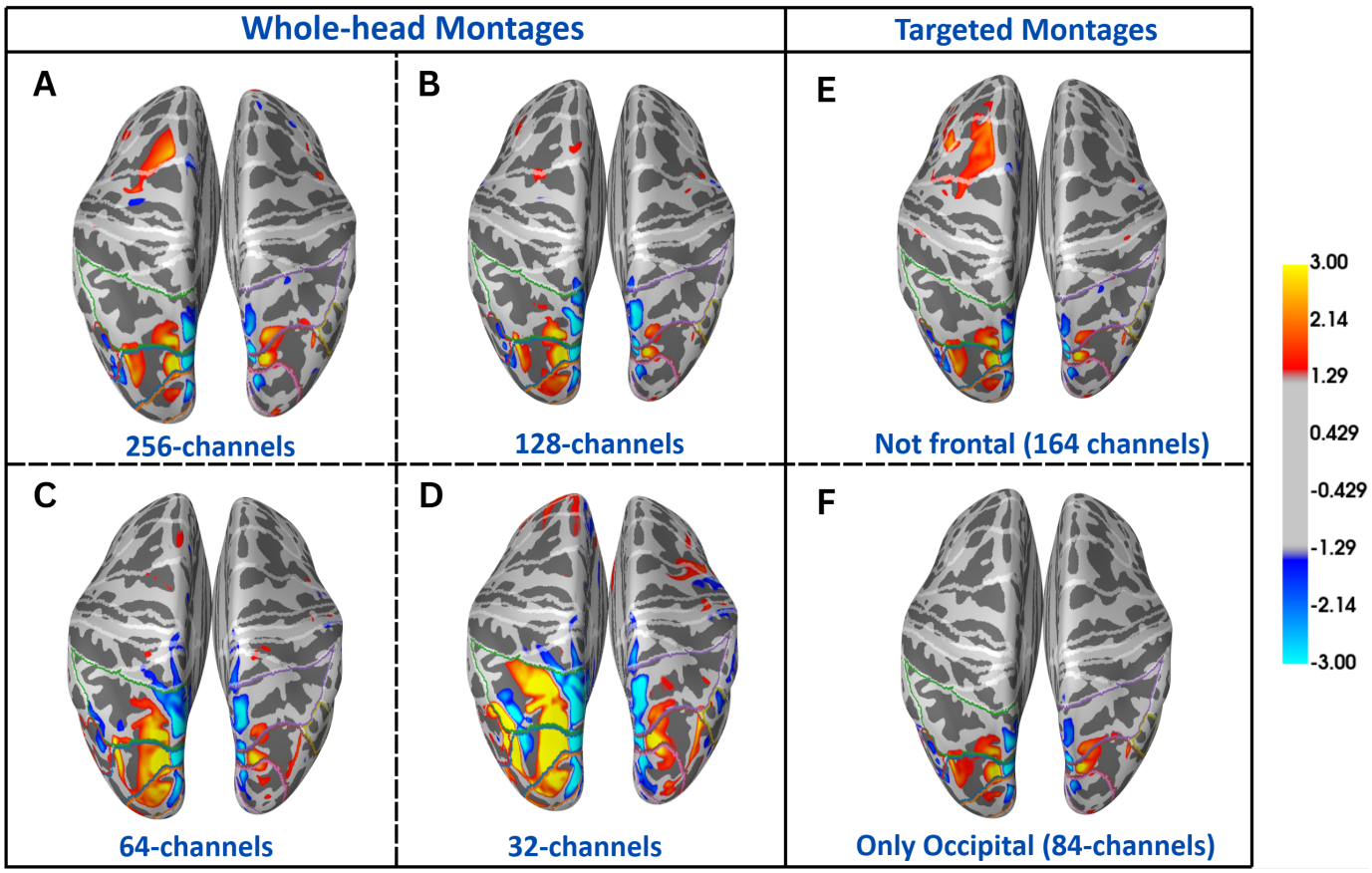

Fig. 15. Dorsal view of source localization results for all montages at the C1 peak (61 ms) during right-hemifield stimulation for the same participant as in Figures 5, 6, 11 and 13. The color bar on the right reports unitless sLORETA values. The side-by-side montage comparison illustrates how altering the electrode density of the ROI changes the spatial extent and focality of the reconstructed occipital activation.